Time-optimized atomic lensing mechanism for the source preparation of dual-species atomic gases in an atom-interferometric test of the weak equivalence principle

Qi Wang [1,2] Junjie Jiang,[1,2] Rundong Xu,[1,2] Lin Zhou [1,3,*] Shi-Guo Peng [1,†] Jin Wang,[1,3,4,‡] and Mingsheng Zhan [1,3,4]

[1]*State Key Laboratory of Magnetic Resonance and Atomic and Molecular Physics, Innovation Academy for Precision Measurement Science and Technology, Chinese Academy of Sciences, Wuhan 430071, China*

[2]*School of Physical Sciences, University of Chinese Academy of Sciences, Beijing 100049, China*

[3]*Hefei National Laboratory, Hefei 230088, China*

[4]*Wuhan Institute of Quantum Technology, Wuhan 430206, China*

In the atom-interferometric test of the weak equivalence principle (WEP) with multicomponent atomic gases, the difference in the center-of-mass positions between different components, as well as the difference in the center-of-mass velocities, leads to systematic uncertainties. An effective way to reduce these systematic uncertainties is to suppress such differences at the preparation stage of atomic sources. In this work, we propose an efficient strategy for preparing two-component gases with a perfectly spatial overlap of the center-of-mass positions and that of the velocities, according to a scheme of the time-optimized atomic lensing mechanism. The key of the time-optimized atomic lensing lies in a two-step quench process of the trap frequency, which is accessible in free-fall experiments by appropriately manipulating the trapping frequency and the center position of the trap. By taking a dual-species rubidium atomic gas as an example, our calculations indicate that the differences in the center-of-mass positions and velocities between ^{85}Rb and ^{87}Rb atoms are simultaneously eliminated, which provides an optimized starting point to test the WEP. An estimation of the systematic uncertainties is also presented. Our method can serve as a potential protocol for the preparation of atom sources in tests of the WEP with multicomponent atomic gases.

I. INTRODUCTION

The weak equivalence principle (WEP), the irrelevance of the trajectory of a freely falling "test" body to its internal structure and composition, is one of the fundamental parts of the equivalence principle, which is one of the basic assumptions of Einstein' s theory of general relativity. Almost all theoretical attempts that try to unify gravity and the standard model require the violation of the equivalence principle [1]. Therefore, it is important to explore the applicable extent of the WEP, which may give birth to new quantum gravity theories. The test of the WEP with atoms [2–12] is as important as that with macroscopic objects [13–17], and it usually relies on the technique of atom interferometries, which was developed about three decades ago [18].

Tests of the WEP with atoms concern not only the factor of the violation of the WEP resulting from the mass [2–8] but also possible factors of those resulting from quantum statistics [9], spin [10,11], superposition [11], internal energy [2,11], and mass and energy [12]. An entanglement test using different atomic species was also proposed [19]. Multicomponent atomic gases are widely used in tests of the WEP. As the measurement accuracy of atom interferometers has improved, the

uncertainties of the positions and velocities of atomic gases and the center-of-mass positions and velocities have gradually become the main sources of systematic errors [20–22]. For example, the center-of-mass position uncertainties of atomic gases must reach the level of nanometers for a WEP test with an accuracy of 10^{-15} [23–25], and uncertainty less than a few micrometers is still required by the compensation method [26]. The noncoincidence between the center-of-mass positions of different components and the difference between their initial center-of-mass velocities lead to additional systematic errors [27]. An impressive amount of effort has been devoted to suppressing the effects originating from those differences [8,12,26,28,29]. Recently, a method to ensure coincidence using magic laser wavelengths for the optical lensing potentials was proposed for specific species [30]. Currently, an ideal preparation of multicomponent atom sources in atom interferometers is crucially needed.

In this work, an efficient strategy based on the so-called atomic lensing mechanism is proposed for the preparation of two-component atomic gases with perfect superpositions of center-of-mass positions and velocities. Delta-kick collimation (DKC) is one of the earliest forms of atomic lensing used to cool atoms. The basic idea of the DKC mechanism lies in the use of a pulsed harmonic potential onto a freely expanding atomic cloud, which acts as a sudden "kick" and brings the system to rest [31,32]. This narrows the momentum distribution of the system and effectively lowers the kinetic temperature as well. It was recently shown that the

*lzhou@wipm.ac.cn

†pengshiguo@wipm.ac.cn

‡wangjin@wipm.ac.cn

delta-kick effect in the DKC mechanics is equivalent to a quench process from a higher trap frequency to a lower one and is just a special case of atomic lensing with unbounded trapping frequencies [33]. For the effect of lowering the effective temperature without atom loss within a short time frame, the atomic lensing mechanism is used to suppress the systematic errors resulting from the uncertainties of momentum distributions (or temperature), such as in the atom-interferometric test of the WEP [8,34] and in gravimeters [35]. Here, taking a dual-species rubidium atomic gas as an example, we develop a time-optimized atomic lensing method by introducing a two-step quench process of the trap frequency, which leads to a perfect superposition of the center-of-mass positions and velocities between two components. Our method can serve as a potential protocol for preparing atom sources in a WEP test with multicomponent atoms. Our analysis shows that the improved atomic lensing mechanism may remarkably increase the coincidence, reduce the expansion speed of atomic gases, and improve the accuracy of the WEP test.

The rest of this paper is arranged as follows. The basic theory of the atomic lensing mechanism is briefly reviewed in the next section. Then the key idea of the time-optimized DKC mechanism for a dual-species atomic gas is presented in Sec. III. We propose a potential experimental protocol for preparing a dual-species rubidium atomic gas by using the time-optimized DKC scheme in Sec. IV. The estimation of systematic uncertainties is analyzed in Sec. V. In Sec. VI, the interaction effect is discussed. Our main results are summarized in Sec. VII.

II. THEORY OF COOLING BY ATOMIC LENSING MECHANICS WITH BOUNDED TRAPPING FREQUENCIES

The process of cooling through an atomic lensing mechanism is utilized to narrow the momentum distribution of atoms, thereby effectively lowering the effective temperature of the system. It relies on the unitary dynamics governed by a time-dependent Hamiltonian. For this reason, we briefly review and discuss the basic theory for describing the dynamics of noninteracting atomic gases in a time-dependent external potential in the presence of gravity. In WEP-test experiments with cold atoms [4,12], the kinetic energy dominates the system, while the collision between atoms in a dilute gas occurs locally, which preserves the conservation of energy and momentum in the instants before and after the collision. As a result, the interaction effect can reasonably be ignored. At low temperature close to the critical temperature, the interatomic interaction may come into play, which we discuss later.

Let us consider a noninteracting gas initially prepared at equilibrium in a harmonic trap with frequency ω_0. The atomic cloud is then made to evolve through the adjustment of the trap characterized by a time-dependent frequency $\omega(t)$. For an individual atom, its motion is governed by the Hamiltonian (the vertical downward direction is taken to be the positive direction in our expressions)

$$H(q, p, t) = \frac{p^2}{2m} + \frac{1}{2}m\omega^2(t)[q - q_0(t)]^2 - mgq, \quad (1)$$

where p and q are, respectively, the momentum and position of the atom, m is the atomic mass, g is the acceleration of gravity, and $q_0(t)$ is the central position of the trap. Here, we consider only a one-dimensional configuration defined along the z direction without loss of generality. It is a convenient choice for the experiment with the WEP test. Since the trap frequency $\omega(t)$ and the trap center $q_0(t)$ vary in time, the atomic cloud is expected to be displaced and to change size simultaneously. For this reason, a canonical scale transformation is introduced [36], i.e.,

$$Q = \frac{q - q_{\text{cm}}(t)}{b(t)}, \quad (2)$$

$$P = b(t)\left(p - m\frac{dq_{\text{cm}}}{dt}\right) - m\frac{db}{dt}(q - q_{\text{cm}}), \quad (3)$$

$$\varsigma = \int \frac{dt}{b^2(t)}, \quad (4)$$

under which the Hamiltonian (1) is equivalently transformed into a time-independent form:

$$H'(P, Q) = \frac{P^2}{2m} + \frac{1}{2}m\omega_0^2 Q^2 + F(\varsigma). \quad (5)$$

The requirement of equivalence between $H(q, p, t)$ and $H'(P, Q)$ under the scale transformation simply yields the equations satisfied by $q_{\text{cm}}(t)$ and $b(t)$, i.e.,

$$\frac{d^2 b}{dt^2} + \omega^2(t)b(t) = \frac{\omega_0^2}{b^3(t)}, \quad (6)$$

$$\frac{d^2 q_{\text{cm}}}{dt^2} + \omega^2(t)\left[q_{\text{cm}}(t) - q_0(t) - \frac{g}{\omega^2(t)}\right] = 0, \quad (7)$$

with the initial conditions $b(0) = 1$, $\dot{b}(0) = 0$, $q_{\text{cm}}(0) = q_0(0)$, and $\dot{q}_{\text{cm}}(0) = 0$. Here, the choice of the function $F(\varsigma)$ in $H'(P, Q)$ is irrelevant for the dynamics, which introduces nothing but an additional gauge phase in the wave function of the atom [36]. One easily finds that $b(t)$ describes the ratio of the temporal atomic cloud size to the initial size, while the center-of-mass position of the cloud is characterized by $q_{\text{cm}}(t)$. Similar quantum analogs of Eq. (6) were also found for describing the dynamics of weakly interacting atomic gases [37,38] and an ideal gas in harmonic traps [39].

For the conventional lensing mechanism according to a sudden quench of the trap from a higher frequency ω_0 to a lower one ω_f (as plotted in Fig. 1, method A) [33], Eq. (6) can easily be solved for time $t > 0$ with the initial conditions $b(0) = 1$ and $\dot{b}(0) = 0$, i.e.,

$$b(t) = \sqrt{1 + \left[\left(\frac{\omega_0}{\omega_f}\right)^2 - 1\right]\sin^2(\omega_f t)}. \quad (8)$$

We find that the instantaneous expansion velocity of the cloud vanishes at the moment $t_n = n\pi/2\omega_f$ with integer $n > 0$, i.e., $\dot{b}(t_n) = 0$. The effective temperature is lowered at this moment as [33]

$$\frac{T(t_n)}{T(0)} \equiv \frac{b^2(0)}{b^2(t_n)} = \frac{\omega_f^2}{\omega_0^2}. \quad (9)$$

Therefore, the atomic lensing mechanism provides an efficient method for the preparation of atom sources with low effective
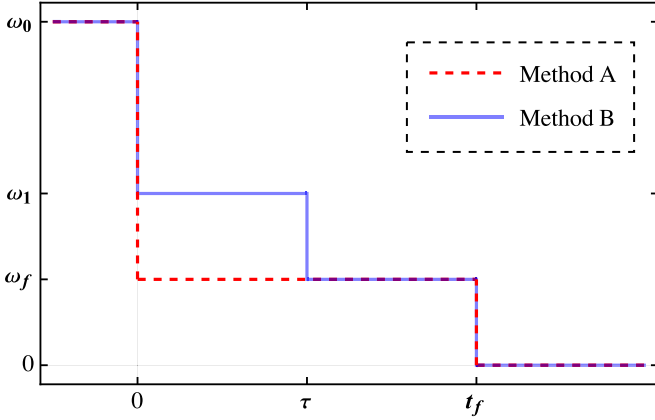
FIG. 1. The schematic of the DKC mechanism according to an appropriate quench process for the trap frequency. Method A illustrates the route of the conventional DKC technique, whereas method B is that of the improved DKC mechanism introduced in this work.

temperature according to an appropriately chosen time of the lens t_f in experiments with atom interferometers [34,40–43].

III. TIME-OPTIMIZED ATOMIC LENSING CONTROL FOR TWO-COMPONENT ATOMIC GASES

For WEP test experiments with two-component atomic gases, the perfect spatial overlap of atomic clouds between different components before release is crucial for suppressing the systematic uncertainties. Specifically speaking, it requires the coincidence of the center-of-mass positions and the center-of-mass velocities between different atomic components. In this section, we introduce an improved time-optimal atomic lensing mechanism at the preparation stage of atomic sources, which may efficiently remove the differences in the center-of-mass positions and velocities of different atomic components. The key to the improved time-optimal atomic lensing mechanism lies in a two-step quench process of the trap frequency: the quench from the initial trap frequency ω_0 to an intermediate one ω_1 at time $t = 0$, followed by an additional quench to the final trap frequency ω_f after evolution time τ. The release time t_f is appropriately chosen for the free-fall experiment after the two-step quench process. A schematic of the time sequence of the improved time-optimal atomic lensing mechanism is presented in Fig. 1 as method B.

To demonstrate the advantage of the improved time-optimized lensing mechanism for the preparation of atom sources, let us consider the experiment configuration of the WEP test by using a dual-species ^{85}Rb and ^{87}Rb atomic gas [4,12]. The atoms are first prepared for $t < 0$ in an initial harmonic trap centered at $q_0(t < 0) = z_0$. However, the trap frequencies experienced by different atomic components are generally not the same and are denoted by $\omega_0^{(s)}$, and $s = 85, 87$ stands for the species of Rb atoms. The equilibrium center-of-mass position of the atoms is at $q_{cm,0}^{(s)} = z_0 + g/\omega_0^{(s)2}$. Subsequently, the trap frequency is abruptly quenched to $\omega_1^{(s)}$, while the trap center is accordingly changed to z_1. The solution of Eq. (7) simply gives the evolution of the center-of-mass

position of species-s atoms in the duration time $0 \leqslant t < \tau$,

$$q_{cm}^{(s)}(t) = d_1^{(s)} \cos\left(\omega_1^{(s)} t\right) + q_{cm,1}^{(s)}, \tag{10}$$

with $d_1^{(s)} = q_{cm,0}^{(s)} - q_{cm,1}^{(s)}$ and $q_{cm,f}^{(s)} = z_1 + g/\omega_1^{(s)2}$. At time $t = \tau$, the trap frequency is further quenched to $\omega_f^{(s)}$, and the trap center is shifted to z_f. Then we obtain

$$q_{cm}^{(s)}(t) = q_{cm,f}^{(s)} + \left[d_2^{(s)} + d_1^{(s)} \cos\left(\omega_1^{(s)} \tau\right)\right] \cos[\omega_f(t - \tau)]$$
$$- \frac{d_1^{(s)} \omega_1^{(s)} \sin\left(\omega_1^{(s)} \tau\right)}{\omega_f} \sin[\omega_f(t - \tau)], \tag{11}$$

with $d_2^{(s)} = q_{cm,1}^{(s)} - q_{cm,f}^{(s)}$ and $q_{cm,f}^{(s)} = z_f + g/\omega_f^{(s)2}$ for $\tau \leqslant t < t_f$. When requiring the coincidence of the center-of-mass positions of two species and their center-of-mass velocities right at the moment $t = t_f$ before the free-fall experiment, we obtain two constraints on the choice of quench times τ and t_f and the corresponding trap center positions z_1 and z_f at each quench, i.e.,

$$q_{cm}^{(85)}(t_f) = q_{cm}^{(87)}(t_f), \quad \dot{q}_{cm}^{(85)}(t_f) = \dot{q}_{cm}^{(87)}(t_f). \tag{12}$$

In addition, the evolution of the atomic cloud size for each species during the two-step quench process is governed by Eq. (6), which determines the final effective temperature before the free-fall experiment. By solving Eq. (6) for the two-step quench dynamics, we easily obtain

$$b_1^{(s)}(t) = \sqrt{1 + \left[\left(\frac{\omega_0^{(s)}}{\omega_1^{(s)}}\right)^2 - 1\right] \sin^2\left(\omega_1^{(s)} t\right)} \tag{13}$$

for $0 < t < \tau$ and

$$b_2^{(s)}(\delta t) = \left\{ \left[b_1^{(s)}(\tau) \cos\left(\omega_f^{(s)} \delta t\right) + \frac{\dot{b}_1^{(s)}(\tau)}{\omega_f^{(s)}} \sin\left(\omega_f^{(s)} \delta t\right) \right]^2 \right.$$
$$\left. + \left[\frac{\omega_0^{(s)}}{b_1^{(s)}(\tau) \omega_f^{(s)}} \right]^2 \sin^2\left(\omega_f^{(s)} \delta t\right) \right\}^{1/2} \tag{14}$$

for $\tau \leqslant t < t_f$ and $\delta t = t - \tau$. Consequently, we may define the effective temperature of the system at $t = t_f$ as the average of those of two species, i.e., $\bar{T} = \sum_{s=85,87} T^{(s)}(t_f)/2$, where $T^{(s)}(t_f)$ is the effective temperature defined by Eq. (9) for the species-s component.

An ideal source of the WEP test requires the center-of-mass positions, center-of-mass velocities, and the widths of the position and velocity distributions of the different components to be matched [44]. Here, we focus on the influence of the center-of-mass positions and the center-of-mass velocities. As the effective temperatures of the gases decrease, the widths of their velocity distributions reduce, as do the uncertainties in their velocities. So we take the optimized choice of (τ, t_f, z_1, z_f), leading to an expected effective temperature $\bar{T}$ that is as low as possible before the free-fall experiment under the constraints (12) that remove the differences in center-of-mass positions and velocities between different species. This can be evaluated as an implicitly constrained optimization problem [45] as follows. For an initial guess of (z_1, z_f), the quench times τ and t_f are solved from Eq. (12). The effective
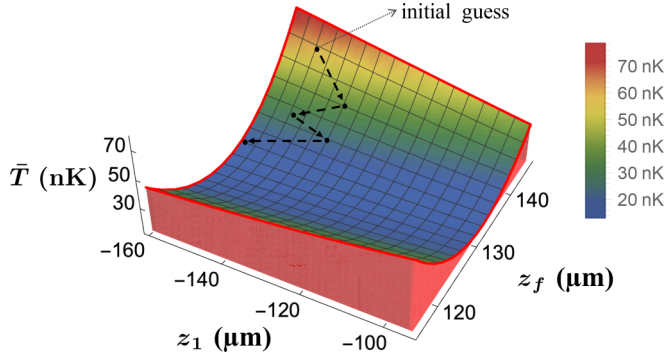
FIG. 2. The schematic of the numerical solution of implicitly constrained optimization problems using the gradient method.

temperature $\bar{T}(z_1, z_f)$ and its gradient are then obtained in the (z_1, z_f) plane, which provides a reasonable guess of (z_1, z_f) for the next step. The optimized solution can be searched according to an iteration process once the effective temperature $\bar{T}$ is as low as possible. Our numerical method is schematically illustrated in Fig. 2.

The differences in the center-of-mass positions $\delta z(t) \equiv | q_{\text{cm}}^{(85)}(t) - q_{\text{cm}}^{(87)}(t) |$ and velocities $\delta v(t) \equiv | \dot{q}_{\text{cm}}^{(85)}(t) - \dot{q}_{\text{cm}}^{(87)}(t) |$ between two components in the two-step atomic lensing process are presented in Fig. 3 (method B). We

find that the differences in the center-of-mass positions and velocities between ^{85}Rb and ^{87}Rb atoms are simultaneously eliminated at time $t = t_f$, which provides an optimized starting point for the WEP test. For comparison, the results of a conventional lensing method are also shown in Fig. 3 (method A). It can be seen that the differences in the center-of-mass positions $\delta z(t)$ and velocities $\delta v(t)$ between two species cannot be removed simultaneously. The starting point for the WEP test according to the conventional lensing method is usually chosen to be time $t = t_f$, when the difference in center-of-mass velocities between two species vanishes [46]. However, the difference in center-of-mass positions may lead to additional systematic errors.

In this calculation, we assume that the sizes of the two components are both 10 μm, and the temperatures are $T_0 = 1$ μK at the initial time $t = t_0$. In method A, $t_{f(A)} = 22.3$ ms is chosen when the velocity difference between the two components is eliminated. Thus, the corresponding effective temperature is consequently $\bar{T}_A = 170$ nK. In method B, $t_{f(B)} = 8.6$ ms is chosen to be the starting time for the WEP test with vanishing differences of the center-of-mass positions and velocities between two components, while the corresponding effective temperature at $t = t_{f(B)}$ is $\bar{T}_B = 13$ nK and $T^{(85)}(t_{f(B)}) \simeq T^{(87)}(t_{f(B)}) \simeq \bar{T}_B$. We find that the time-optimized atomic lensing mechanism provides an efficient scheme for the preparation of two-species atomic sources for the WEP test with even lower effective temperature.

IV. EXPERIMENTAL PROTOCOL

The key technique in the time-optimized atomic lensing mechanism lies in the precise and independent manipulation of the trap center and trapping frequency experienced by atoms. This can be achieved by using the technique of a time-averaged optical potential (TOP) trap. Unlike that in Ref. [12], the dual-species atomic gas is loaded into a TOP trap, which is well controlled by a radio-frequency (rf) field through an acousto-optic modulator (AOM) or an acousto-optic deflector (AOD) [47–49]. The center of the TOP trap and the trapping frequency experienced by atoms can independently be adjusted by changing the center frequency of the rf field and its bandwidth separately.

The proposed experimental setup is presented in Fig. 4. The atoms are trapped on the focus plane of the lens by the dipole force of the laser beam. In the presence of an AOD (AOM) driven by a rf field, the optical potential experienced by atoms on the focus plane is modulated by the frequency of the rf field, which effectively results in a time-averaged trapping potential for atoms. Consequently, the trap center is controlled by the center frequency of the rf field, while the trapping frequency is independently manipulated by the bandwidth of the rf field. Continuing to lower the trap frequency ω_f can further decrease the effective temperature T, i.e., Eq. (9). When the trapping frequency is too low to confine the atoms, compensating for the effects of gravity in the TOP trap with a linear potential becomes necessary [49]. Recently, by combing the technique of the TOP and atomic lensing mechanism, Ref. [42] reported that an atomic gas with an effective temperature of 40 nK was acquired.
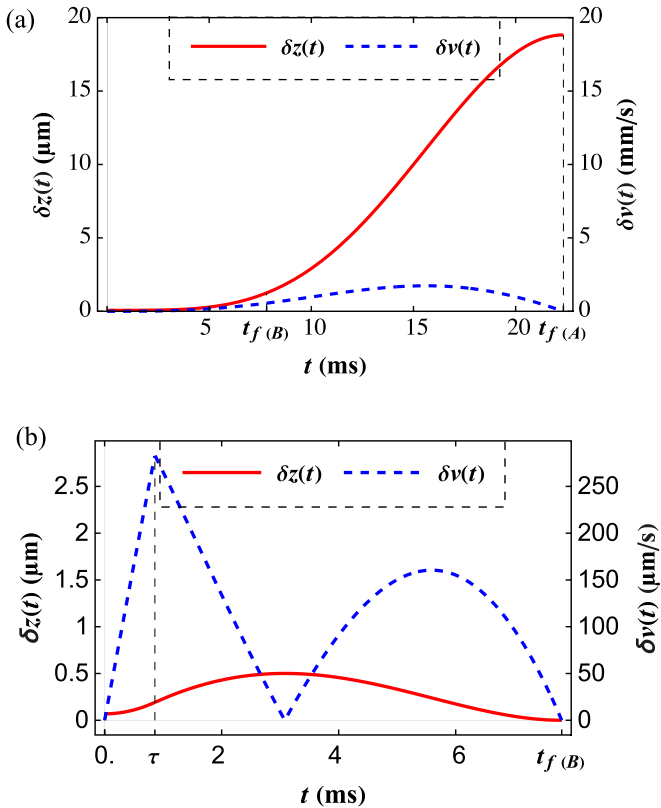

FIG. 3. The position difference $\delta z(t)$ of the center of mass of the two-component gases as a function of time (solid red line) and the velocity difference $\delta v(t)$ as a function of time (dashed blue line) for (a) method A and (b) Method B. Here, the parameters are chosen to be $\omega_0/2\pi = 286.5$ Hz, $\omega_1/2\pi = 47.7$ Hz, and $\omega_f/2\pi = 31.8$ Hz.
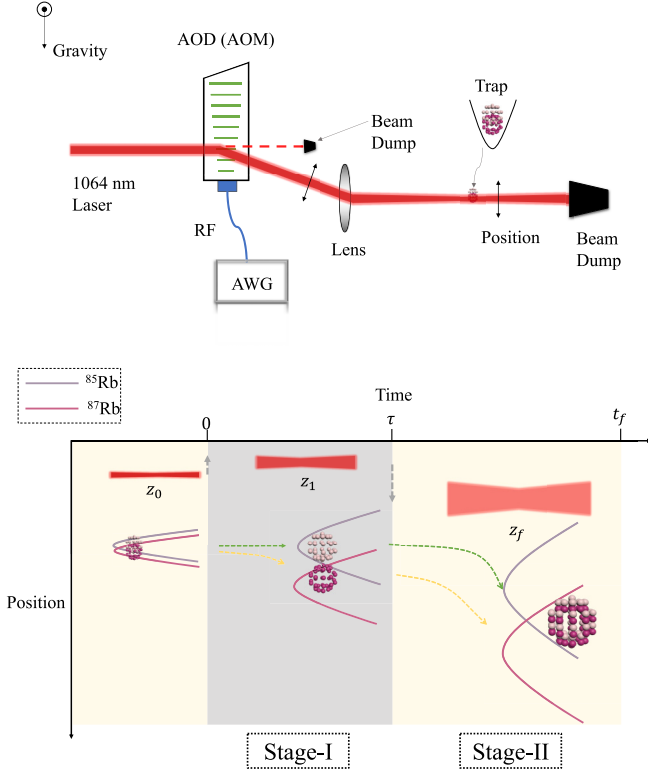
FIG. 4. Schematic of the optical trap setup and experimental process. The position of the center of the trap and the trap frequency are controlled through the AOD (AOM); we can easily change them in different stages by changing the rf frequency. The wave form of the rf is modulated by an arbitrary wave-form generator (AWG).

V. ESTIMATION OF SYSTEMATIC ERRORS

The systematic errors in the WEP tests are determined by all the effects influencing the relative phase of the dual-species atom interferometer, except for the linear part of the gravitational field. Take the gravity-gradient effect, one of the main sources of systematic error, as an example. The systematic error can be caused by the center-of-mass position difference Δz and the center-of-mass velocity difference Δv through the gravity-gradient effect, resulting in an acceleration difference [12]

$$\Delta g = \Gamma_{zz}(\Delta z + \Delta v T_{\text{MZ}}), \quad (15)$$

where Γ_{zz} is the first order of gravity gradients and T_{MZ} is half of the interrogation time of the Mach-Zehnder atom interferometer. In our recent work [12], the uncertainty of the position difference in the molasses was 0.79 mm; the corresponding uncertainty of the test was 2.8×10^{-10}, which was the largest term in the test. The uncertainty of the velocity difference was controlled below $100\,\mu\text{m/s}$ by the selection of Raman pules; the corresponding uncertainty of the test was 6×10^{-12}.

In order to assess the practical feasibility of our method, the impact of small experimental imperfections needs to be estimated. Although $\Delta z = \delta z(t_{f(B)}) = 0$ and $\Delta v = \delta v(t_{f(B)}) = 0$ in method B under ideal conditions, the uncertainties of Δz and Δv can be caused by position errors of the trap centers, time errors, the fluctuation of laser power, and the anhar-

monicities of traps during the experiments. We consider them all independently and give the results in Fig. 5.

Under laboratory conditions, the time (the relative position) controlled by the AOD (AOM) can be easily determined to the 1-μs (0.1-μm) level. Correspondingly, the determination of the initial center-of-mass position is to the 1-nm level. However, the determination of the initial center-of-mass position to the 1-nm level in one shot requires χ below 10^{-3}, which leads to high demands for the stability of laser intensity. It is easy to get $\chi = \sqrt{10^{-3}}$, corresponding to a 0.1% fluctuation of the laser intensity in experiments; then we can get the uncertainty of the center-of-mass position difference $\delta\Delta z = 39$ nm and the uncertainty of the center-of-mass velocity difference $\delta\Delta v = 32\,\mu\text{m/s}$ in one shot according to Fig. 5. And we can reduce the uncertainty of Δz and Δv by repeating the experiment several times. If we take the the number of measurements $\nu = 10^4$, the uncertainty of the center-of-mass position difference is below 1 nm, and the uncertainty of the center-of-mass velocity difference is below $1\,\mu\text{m/s}$, which meet the requirements of a WEP test with a resolution of 10^{-15} [26].

The other effects, like the wave-front distortion of laser beams and Coriolis effect, are more related to the difference in the horizon. Also, we can use the atomic lens in the orthogonal horizontal transverse direction. The uncertainty caused by the wave-front distortion can be suppressed to 10^{-13} with our expansion-rate-selection method [50], and the uncertainty related to the Coriolis effect can be reduced to 10^{-13} by compensating for the rotation of the Raman laser's mirror with an accuracy of 10 nrad/s [51]. In conclusion, the joint mass-energy test of the WEP is expected to be 10^{-12}–10^{-13}[52].

VI. INTERACTION EFFECT

Previously, we discussed the time-optimized atomic lensing technique for ideal gases. While the time-optimized atomic lensing mechanism may dramatically reduce the effective temperature of a system, interatomic interactions might come into play. In this section, we estimate the effect of interactions between atoms. To start, let us consider the distribution function $f(\mathbf{r}, \mathbf{v}, t)$ of the system in phase space, which obeys the Boltzmann equation [53,54]

$$\frac{\partial f}{\partial t} + \mathbf{v} \cdot \frac{\partial f}{\partial \mathbf{r}} - \frac{1}{m}\frac{\partial U}{\partial \mathbf{r}} \cdot \frac{\partial f}{\partial \mathbf{v}} - 2\frac{g_{\text{int}}}{m}\frac{\partial n}{\partial \mathbf{r}} \cdot \frac{\partial f}{\partial \mathbf{v}} = 0, \quad (16)$$

where $U(\mathbf{r}, t) = \sum_i m\omega_i^2(t)r_i^2/2 - mgz$ is the external potential, g_{int} is the interaction strength, and $n = \int f(\mathbf{r}, \mathbf{v}, t)d\mathbf{v}$ is the density profile. Here, the dissipation of the system is ignored. At equilibrium, i.e., $\partial f/\partial t = 0$, we obtain an equation satisfied by the distribution function $f_0(\mathbf{r}, \mathbf{v})$ at equilibrium,

$$\sum_i \left(v_i \frac{\partial f_0}{\partial r_i'} - \omega_0^2 r_i' \frac{\partial f_0}{\partial v_i} - \frac{2g_{\text{int}}}{m}\frac{\partial n_0}{\partial r_i'}\frac{\partial f_0}{\partial v_i} \right) = 0, \quad (17)$$

where we have redefined the coordinates as $x' = x, y' = y$, and $z' = z - g/\omega_z^2(t)$. At nonequilibrium, the distribution function is assumed to take the scaling form of $f(\mathbf{r}', \mathbf{v}, t) = f_0(\mathbf{R}(t), \mathbf{V}(t))$, with $R_i = r_i'/b_i$ and $V_i = b_i v_i - \dot{b}_i r_i'$ [53,54].
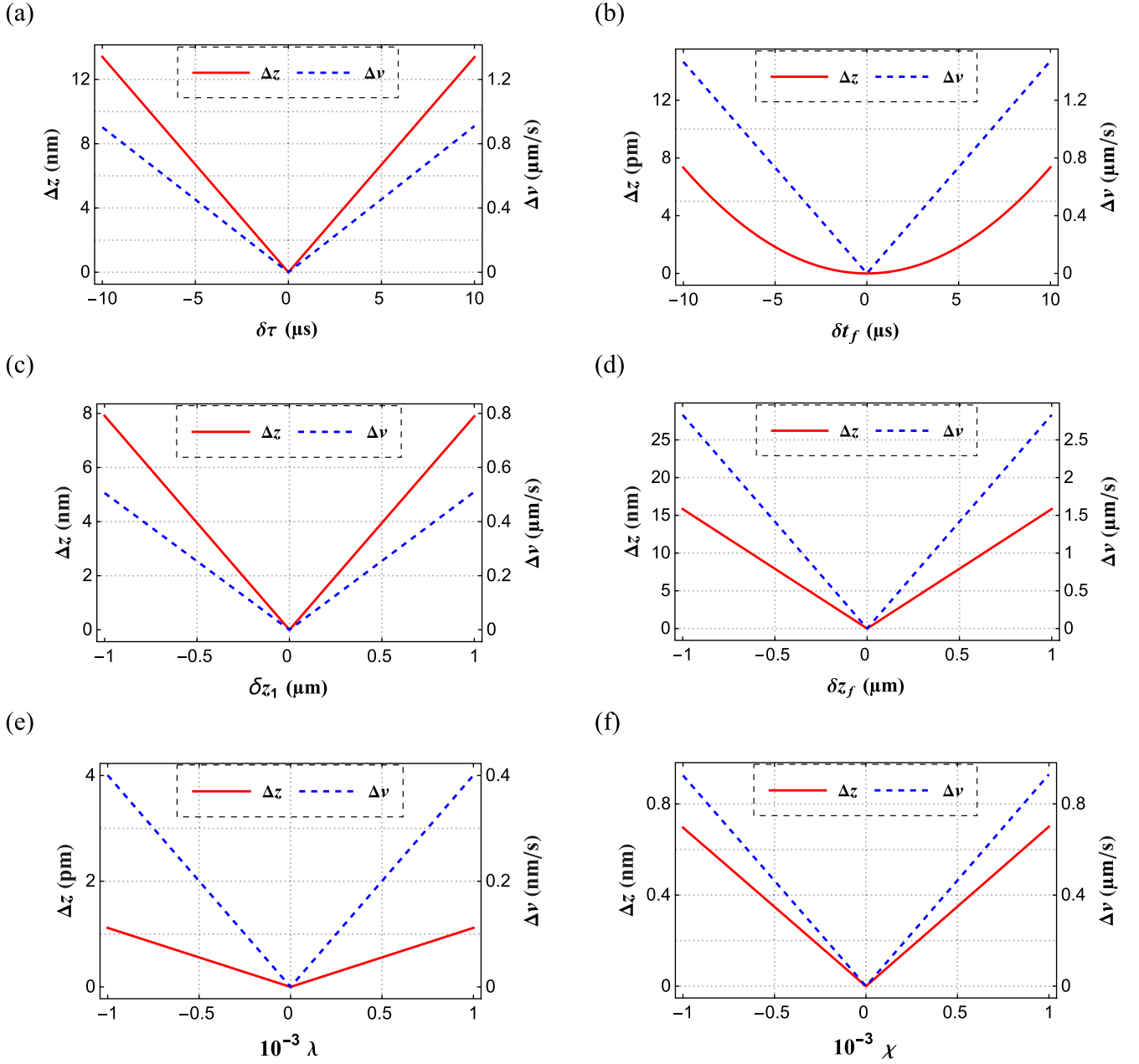
(a)

(b)

(c)

(d)

(e)

(f)

FIG. 5. Δz is represented by the red solid line, and Δv is represented by the blue dashed line. (a) The duration of the first pulse is described by $\tau' = \tau + \delta\tau$, and $\delta\tau$ describes the time error in the first stage. (b) The duration of the second pulse is described by $t'_f = t_f + \delta t_f$, and δt_f describes the time error in the second stage. (c) The relative position of the initial trap and the trap of the first pulse is described by $z'_1 = z_1 + \delta z_1$, and δz_1 describes the position error in the first stage. (d) The relative position of the initial trap and the trap of the first pulse is described by $z'_f = z_f + \delta z_f$, and δz_f describes the position error in the second stage. (e) The potential is described by $U_{(s)}(z) = \frac{1}{2}m_{87}\omega^2_{87(s)}z^2 - \lambda m_{87}\omega^2_{87(s)}z^3$, and λ describes the anharmonicities. (f) The trap frequency is described by $\omega'_{(s)} = (1 + \chi)\omega_{(s)}$, which is mainly affected by the laser power fluctuation. The chosen parameters are $\omega_0/2\pi = 286.5$ Hz, $\omega_1/2\pi = 47.7$ Hz, and $\omega_f/2\pi = 31.8$ Hz.

Inserting the scaling ansatz into Eq. (16), we get

$$\sum_i \left\{ \frac{V_i}{b_i^2} \frac{\partial f_0}{\partial R_i} - b_i R_i \left(\ddot{b}_i + \omega_i^2 b_i \right) \frac{\partial f_0}{\partial V_i} - \frac{2g_{\text{int}}}{m\Pi b_j} \frac{\partial n_0}{\partial R_i} \frac{\partial f_0}{\partial V_i} \right\} = 0. \tag{18}$$

We find that the time dependence of the distribution function is entirely contained in the scaling factor $b_i(t)$. Multiplying both sides of Eq. (18) by $R_i V_i$ and integrating over **R** and **V**,

i.e., $\int R_i V_i [\cdots] d\mathbf{R} d\mathbf{V}$, we finally obtain the equation satisfied by the scaling factor

$$\ddot{b}_i + \omega_i^2(t) b_i = \omega_0^2 \left(\frac{1-\xi}{b_i^3} + \frac{\xi}{b_i \Pi_j b_j} \right), \tag{19}$$

with

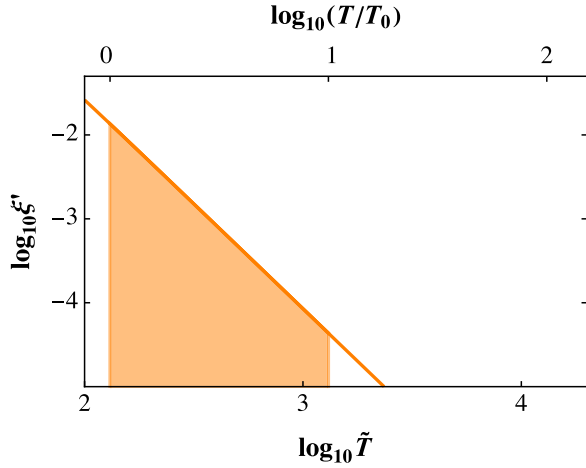$$\xi = \frac{E_{mf}}{E_{mf} + k_B T}, \tag{20}$$

FIG. 6. The interaction effect characterized by the parameter ξ' as a function of the reduced temperature $\tilde{T} = k_B T / \hbar \omega_0$. Here, the typical parameters are chosen to be $\omega_0 / 2\pi = 286.5$ Hz, $T_0 = 1$ μK, and $N = 1.0 \times 10^6$. The ^{85}Rb scattering length is $a_{85} = -443 a_0$, the ^{87}Rb scattering length is $a_{87} = 99 a_0$, the interspecies scattering length is $a_{87-85} = 213 a_0$, and a_0 is Bohr's radius [56].

where $E_{mf} = g_{\text{int}} \int n_0^2(\mathbf{r}) d\mathbf{r}$ is the mean-filed interaction energy at the initial equilibrium state and T is the temperature. Equation (19) simply reduces to Eq. (6) in the noninteracting limit with $\xi = 0$. Therefore, the interaction effect is characterized by parameter ξ of the initial state with the density profile $n_0(\mathbf{r})$, which simply takes the Gaussian form

$$n_0(\mathbf{r}) = \frac{N \exp\left(-\sum_{i=1}^{3} r_i^2 / 2\sigma_{0,i}^2\right)}{(2\pi)^{3/2} \prod_{i=1}^{3} \sigma_{0,i}}, \tag{21}$$

with the spatial extension $\sigma_{0,i}$ along the ith direction and N being the total number of atoms. Then we find

$$\xi = \left[1 + \frac{2\sqrt{\pi} a_{ho}}{aN} \left(\frac{k_B T}{\hbar \omega_0} \right)^{5/2} \right]^{-1}, \tag{22}$$

where $a_{ho} = \sqrt{\hbar / \omega_0}$ is the harmonic length with respect to the initial trap and a is the scattering length between atoms.

For a dual-species atomic gas, the total interaction energy is accordingly expressed as [55]

$$E_{\text{total}} = N \int_V \left[\frac{1}{2} g_{87} n_{87}^2 + g_{87-85} n_{87} n_{85} + \frac{1}{2} g_{85} n_{85}^2 \right] d\mathbf{r}. \tag{23}$$

Then we have

$$\xi' = \frac{E_{\text{total}}}{E_{\text{total}} + k_B T} = \frac{1}{1 + \frac{\sqrt{\pi} a_{ho}}{N} \left(\frac{1}{a_{87}} + \frac{2}{a_{87-85}} + \frac{1}{a_{85}} \right) \tilde{T}^{\frac{5}{2}}}. \tag{24}$$

The estimation of the interaction effect ξ' as a function of the reduced temperature is presented in Fig. 6. The shaded area is the typical region of the reduced temperature for experiments with the WEP test [12]. We find that the interaction effect is extremely small when the temperature of the system is well above the transition temperature of Bose-Einstein condensation in our method. Thus, we may reasonably ignore the interatomic interactions in the analysis of the estimation of the systematic uncertainty.

VII. CONCLUSIONS

The two-component sources of atom interferometers can be made to coincide in the center-of-mass positions and velocities in a shorter amount of time directly by changing the trap frequency and trap center during the atomic lensing process, and this process reduces the effective temperatures of the atomic gases effectively. Optimized atomic sources with a lower effective temperature are critical for future experiments. These sources can significantly reduce systematic errors, shorten preparation time, and ensure long-term uncertainty limits are reached faster in WEP tests. Furthermore, reducing additional processes, such as the adjustment of atomic positions using Raman pluses, not only reduces the preparation time of the sources but also avoids the heating of the atoms and the loss of the effective atomic number for the atom interferometer. Although the nanokelvin level of the effective temperatures in our protocol is sufficient for experiments currently, picokelvin-scale effective temperatures are needed for future experiments and were discussed in [40,41,57–59]. In our method, the interactions are small enough to ignore. Actually, even if the initial temperature is so low that the interactions cannot be ignored, we can add a free expansion stage or invert the trap [33] before stage I to reduce the interactions. Although the additional stage introduces additional differences in velocity and position, these differences can be evaluated or measured, and our protocol can effectively eliminate them. This is possible because the constraints outlined in Eq. (12) remain constant.

This work is based on the example of ^{85}Rb and ^{87}Rb gases, but the method can easily be extended to ^{87}Rb‑^{39}K [3], ^{88}Sr‑^{87}Sr [9], and ^{87}Rb‑^{170}Yb [44] systems, which are not restricted to specific species, and the difference in the center-of-mass positions can be adjusted with accuracy below 1 μm in one shot under the present experimental conditions. This is beneficial to a high-precision WEP test of microparticles at the Zhaoshan long-baseline Atom Interferometer Gravitation Antenna (ZAIGA) [60].

[1] C. M. Will, The confrontation between general relativity and experiment, Living Rev. Relativ. **9**, 3 (2006).

[2] S. Fray, C. A. Diez, T. W. Hänsch, and M. Weitz, Atomic Interferometer with Amplitude Gratings of Light and Its Applications to Atom Based Tests of the Equivalence Principle, Phys. Rev. Lett. **93**, 240404 (2004).

[3] D. Schlippert, J. Hartwig, H. Albers, L. L. Richardson, C. Schubert, A. Roura, W. P. Schleich, W. Ertmer, and E. M. Rasel, Quantum Test of the Universality of Free Fall, Phys. Rev. Lett. **112**, 203002 (2014).

[4] L. Zhou, S. Long, B. Tang, X. Chen, F. Gao, W. Peng, W. Duan, J. Zhong, Z. Xiong, J. Wang, Y. Zhang, and M. Zhan, Test of Equivalence Principle at 10^{-8} Level by a Dual-Species Double-Diffraction Raman Atom Interferometer, Phys. Rev. Lett. **115**, 013004 (2015).

[5] B. Barrett, L. Antoni-Micollier, L. Chichet, B. Battelier, T. Lévèque, A. Landragin, and P. Bouyer, Dual matter-wave inertial sensors in weightlessness, Nat. Commun. **7**, 13786 (2016).

[6] H. Albers, A. Herbst, L. L. Richardson, H. Heine, D. Nath, J. Hartwig, C. Schubert, C. Vogt, M. Woltmann, C. Lämmerzahl, S. Herrmann, W. Ertmer, E. M. Rasel, and D. Schlippert, Quantum test of the universality of free fall using rubidium and potassium, Eur. Phys. J. D **74**, 145 (2020).

[7] K. Zhang, M. K. Zhou, Y. Cheng, L. L. Chen, Q. Luo, W. J. Xu, L. S. Cao, X. C. Duan, and Z. K. Hu, Testing the universality of free fall by comparing the atoms in different hyperfine states with Bragg diffraction, Chin. Phys. Lett. **37**, 043701 (2020).

[8] P. Asenbaum, C. Overstreet, M. Kim, J. Curti, and M. A. Kasevich, Atom-Interferometric Test of the Equivalence Principle at the 10^{-12} Level, Phys. Rev. Lett. **125**, 191101 (2020).

[9] M. G. Tarallo, T. Mazzoni, N. Poli, D. V. Sutyrin, X. Zhang, and G. M. Tino, Test of Einstein Equivalence Principle for 0-Spin and Half-Integer-Spin Atoms: Search for Spin-Gravity Coupling Effects, Phys. Rev. Lett. **113**, 023005 (2014).

[10] X. C. Duan, X. B. Deng, M. K. Zhou, K. Zhang, W. J. Xu, F. Xiong, Y. Y. Xu, C. G. Shao, J. Luo, and Z. K. Hu, Test of the Universality of Free Fall with Atoms in Different Spin Orientations, Phys. Rev. Lett. **117**, 023001 (2016).

[11] G. Rosi, G. D'Amico, L. Cacciapuoti, F. Sorrentino, M. Prevedelli, M. Zych, C. Brukner, and G. M. Tino, Quantum test of the equivalence principle for atoms in coherent superposition of internal energy states, Nat. Commun. **8**, 15529 (2017).

[12] L. Zhou, C. He, S. T. Yan, X. Chen, D. F. Gao, W. T. Duan, Y. H. Ji, R. D. Xu, B. Tang, C. Zhou, S. Barthwal, Q. Wang, Z. Hou, Z. Y. Xiong, Y. Z. Zhang, M. Liu, W. T. Ni, J. Wang, and M. S. Zhan, Joint mass-and-energy test of the equivalence principle at the 10^{-10} level using atoms with specified mass and internal energy, Phys. Rev. A **104**, 022822 (2021).

[13] J. G. Williams, S. G. Turyshev, and D. H. Boggs, Progress in Lunar Laser Ranging Tests of Relativistic Gravity, Phys. Rev. Lett. **93**, 261101 (2004).

[14] F. Hofmann and J. Müller, Relativistic tests with lunar laser ranging, Class. Quantum Grav. **35**, 035015 (2018).

[15] P. Touboul *et al.*, *MICROSCOPE* Mission: First Results of a Space Test of the Equivalence Principle, Phys. Rev. Lett. **119**, 231101 (2017).

[16] S. Schlamminger, K. Y. Choi, T. A. Wagner, J. H. Gundlach, and E. G. Adelberger, Test of the Equivalence Principle Using a Rotating Torsion Balance, Phys. Rev. Lett. **100**, 041101 (2008).

[17] L. Zhu, Q. Liu, H. H. Zhao, Q. L. Gong, S. Q. Yang, P. Luo, C. G. Shao, Q. L. Wang, L. C. Tu, and J. Luo, Test of the Equivalence Principle with Chiral Masses Using a Rotating Torsion Pendulum, Phys. Rev. Lett. **121**, 261101 (2018).

[18] A. D. Cronin, J. Schmiedmayer, and D. E. Pritchard, Optics and interferometry with atoms and molecules, Rev. Mod. Phys. **81**, 1051 (2009).

[19] R. Geiger and M. Trupke, Proposal for a Quantum Test of the Weak Equivalence Principle with Entangled Atomic Species, Phys. Rev. Lett. **120**, 043602 (2018).

[20] L. Morel, Z. Yao, P. Cladé, and S. Guellati-Khélifa, Determination of the fine-structure constant with an accuracy of 81 parts per trillion, Nature (London) **588**, 61 (2020).

[21] G. Rosi, F. Sorrentino, L. Cacciapuoti, M. Prevedelli, and G. M. Tino, Precision measurement of the Newtonian gravitational constant using cold atoms, Nature (London) **510**, 518 (2014).

[22] R. H. Parker, C. Yu, W. Zhong, B. Estey, and H. Müller, Measurement of the fine-structure constant as a test of the standard model, Science **360**, 191 (2018).

[23] S. Dimopoulos, P. W. Graham, J. M. Hogan, and M. A. Kasevich, General relativistic effects in atom interferometry, Phys. Rev. D **78**, 042003 (2008).

[24] D. N. Aguilera, H. Ahlers, B. Battelier *et al.*, STE-QUEST—Test of the universality of free fall using cold atom interferometry, Class. Quantum Gravity **31**, 115010 (2014).

[25] A. Bassi, L. Cacciapuoti, S. Capozziello *et al.*, A way forward for fundamental physics in space, npj Microgravity **8**, 49 (2022).

[26] A. Roura, Circumventing Heisenberg's Uncertainty Principle in Atom Interferometry Tests of the Equivalence Principle, Phys. Rev. Lett. **118**, 160401 (2017).

[27] A. M. Nobili, Fundamental limitations to high-precision tests of the universality of free fall by dropping atoms, Phys. Rev. A **93**, 023617 (2016).

[28] R. Chamakhi, H. Ahlers, M. Telmini, C. Schubert, E. M. Rasel, and N. Gaaloul, Species-selective lattice launch for precision atom interferometry, New J. Phys. **17**, 123002 (2015).

[29] S. Loriani, C. Schubert, D. Schlippert, W. Ertmer, F. Pereira Dos Santos, E. M. Rasel, N. Gaaloul, and P. Wolf, Resolution of the colocation problem in satellite quantum tests of the universality of free fall, Phys. Rev. D **102**, 124043 (2020).

[30] M. Meister and A. Roura, Efficient matter-wave lensing of ultracold atomic mixtures, Quantum Sci. Technol. **8**, 024001 (2023).

[31] H. Ammann and N. Christensen, Delta Kick Cooling: A New Method for Cooling Atoms, Phys. Rev. Lett. **78**, 2088 (1997).

[32] R. Corgier, S. Loriani, H. Ahlers, K. Posso-Trujillo, C. Schubert, E. M Rasel, E. Charron, and N. Gaaloul, Interacting quantum mixtures for precision atom interferometry, New J. Phys. **22**, 123008 (2020).

[33] L. Dupays, D. C. Spierings, A. M. Steinberg, and A. del Campo, Delta-kick cooling, time-optimal control of scale-invariant dynamics, and shortcuts to adiabaticity assisted by kicks, Phys. Rev. Res. **3**, 033261 (2021).

[34] H. Müntinga *et al.*, Interferometry with Bose-Einstein Condensates in Microgravity, Phys. Rev. Lett. **110**, 093602 (2013).

[35] S. Abend, M. Gebbe, M. Gersemann, H. Ahlers, H. Muntinga, E. Giese, N. Gaaloul, C. Schubert, C. Lammerzahl, W. Ertmer,

W. P. Schleich, and E. M. Rasel, Atom-Chip Fountain Gravimeter, Phys. Rev. Lett. **117**, 203003 (2016).

[36] J. F. Schaff, P. Capuzzi, G. Labeyrie, and P. Vignolo, Shortcuts to Adiabaticity for Trapped Ultracold Gases, New J. Phys. **13**, 113017 (2011).

[37] Y. Castin and R. Dum, Bose-Einstein Condensates in Time Dependent Traps, Phys. Rev. Lett. **77**, 5315 (1996).

[38] Y. Kagan, E. L. Surkov, and G. V. Shlyapnikov, Evolution of a Bose-condensed gas under variations of the confining potential, Phys. Rev. A **54**, R1753 (1996).

[39] G. M. Bruun and C. W. Clark, Ideal gases in time-dependent traps, Phys. Rev. A **61**, 061601(R) (2000).

[40] T. Kovachy, J. M. Hogan, A. Sugarbaker, S. M. Dickerson, C. A. Donnelly, C. Overstreet, and M. A. Kasevich, Matter Wave Lensing to Picokelvin Temperatures, Phys. Rev. Lett. **114**, 143004 (2015).

[41] C. Deppner, W. Herr, M. Cornelius, P. Stromberger, T. Sternke, C. Grzeschik, A. Grote, J. Rudolph, S. Herrmann, M. Krutzik, A. Wenzlawski, R. Corgier, E. Charron, D. Guéry-Odelin, N. Gaaloul, C. Lämmerzahl, A. Peters, P. Windpassinger, and E. M. Rasel, Collective-Mode Enhanced Matter-Wave Optics, Phys. Rev. Lett. **127**, 100401 (2021)

[42] H. Albers, R. Corgier, A. Herbst, A. Rajagopalan, C. Schubert, C. Vogt, M. Woltmann, C. Lämmerzahl, S. Herrmann, E. Charron, W. Ertmer, E. M. Rasel, N. Gaaloul, and D. Schlippert, All-optical matter-wave lens using time-averaged potentials, Commun. Phys. **5**, 60 (2022).

[43] D. Becker, M. D. Lachmann, S. T. Seidel *et al.*, Space-borne Bose–Einstein condensation for precision interferometry, Nature (London) **562**, 391 (2018).

[44] J. Hartwig, S. Abend, C. Schubert, D. Schlippert, H. Ahlers, K. Posso-Trujillo, N. Gaaloul, W. Ertmer, and E. M. Rasel, Testing the universality of free fall with rubidium and ytterbium in a very large baseline atom interferometer, New J. Phys. **17**, 035011 (2015).

[45] M. Heinkenschloss and L. N. Vicente, An interface optimization and application for the numerical solution of optimal control problems, ACM Trans. Math. Software **25**, 157 (1999).

[46] C. Overstreet, Atom-interferometric test of the equivalence principle and observation of a quantum system in curved space-time, Ph.D. thesis, Stanford University (2020).

[47] R. Roy, A. Green, R. Bowler, and S. Gupta, Rapid cooling to quantum degeneracy in dynamically shaped atom traps, Phys. Rev. A **93**, 043403 (2016).

[48] G. Condon, M. Rabault, B. Barrett, L. Chichet, R. Arguel, H. Eneriz-Imaz, D. Naik, A. Bertoldi, B. Battelier, P. Bouyer, and A. Landragin, All-Optical Bose-Einstein Condensates in Microgravity, Phys. Rev. Lett. **123**, 240402 (2019).

[49] K. Shibata, H. Ikeda, R. Suzuki, and T. Hirano, Compensation of gravity on cold atoms by a linear optical potential, Phys. Rev. Res. **2**, 013068 (2020).

[50] J. G. Hu, X. Chen, J. Fang, L. Zhou, J. Q. Zhong, J. Wang, and M. S. Zhan, Analysis and suppression of wave-front-aberration phase noise in weak-equivalence-principle tests using dual-species atom interferometers, Phys. Rev. A **96**, 023618 (2017).

[51] W. T. Duan, C. He, S. T. Yan, Y. H. Ji, L. Zhou, X. Chen, J. Wang, and M. S. Zhan, Suppression of Coriolis error in weak equivalence principle test using ^{85}Rb - ^{87}Rb dual-species atom interferometer, Chin. Phys. B **29**, 070305 (2020).

[52] L. Zhou, S. T. Yan, Y. H. Ji, C. He, J. J. Jiang, Z. Hou, R. D. Xu, Q. Wang, Z. X. Li, D. F. Gao, M. Liu, W. T. Ni, J. Wang, and M. S. Zhan, Towards higher precision mass-energy test of the equivalence principle with atom interferometers, Front. Phys. **10**, 3389 (2022).

[53] D. Guéry-Odelin, Mean-field effects in a trapped gas, Phys. Rev. A **66**, 033613 (2002).

[54] P. Pedri, D. Guéry-Odelin, and S. Stringari, Dynamics of a classical gas including dissipative and mean-field effects, Phys. Rev. A **68**, 043608 (2003).

[55] D. S. Petrov, Quantum Mechanical Stabilization of a Collapsing Bose-Bose Mixture, Phys. Rev. Lett. **115**, 155302 (2015).

[56] S. B. Papp, J. M. Pino, and C. E. Wieman, Tunable Miscibility in a Dual-Species Bose-Einstein Condensate, Phys. Rev. Lett. **101**, 040402 (2008).

[57] T. van Zoest, N. Gaaloul, Y. Singh *et al.*, Bose-Einstein condensation in microgravity, Science **328**, 1540 (2010).

[58] R. Corgier, S. Amri, W. Herr, A. Ahlers, J. Rudolph, D. Guéry-Odelin, E. M. Rasel, E. Charron, and N. Gaaloul, Fast manipulation of Bose–Einstein condensates with an atom chip, New J. Phys. **20**, 055002 (2018).

[59] N. Gaaloul, M. Meister, R. Corgier, A. Pichery, P. Boegel, W. Herr, H. Ahlers, E. Charron, J. R. Williams, R. J. Thompson, W. P. Schleich, E. M. Rasel, and N. P. Bigelow, A space-based quantum gas laboratory at picokelvin energy scales, Nat. Commun. **13**, 7889 (2022).

[60] M. S. Zhan, J. Wang, W. T. Ni *et al.*, ZAIGA: Zhaoshan long-baseline atom interferometer gravitation antenna, Int. J. Mod. Phys. D **29**, 1940005 (2020).